11th Australasian Fluid Mechanics Conference
University of Tasmania, Hobart, Australia
14-18 December 1992

COMPUTATIONAL SIMULATION OF FLOW ABOUT A COBRA PROBE WITH PURGING

M. DE GUZMAN[1], C.A.J. FLETCHER[1] and J.D. HOOPER[2]

[1]Dept of Mechanical Engineering, University of Sydney, NSW 2006, AUSTRALIA

[2]CSIRO Division of Mineral & Process Engineering, PMB 5, Menai, NSW 2234, AUSTRALIA

ABSTRACT

The flow behaviour around a four-hole Cobra probe , suitable for complex, three dimensional, single-phase flow, is investigated computationally. Velocity components and pressure adjacent to the probe tip are presented for pitch and yaw angles up to $\alpha_p = 42^o$, $\beta_y = 48^o$. Agreement with calibration pressures is good except on leeward faces when both α_p and β_y are large. For $\alpha_p = 0^o$, $\beta_y = 20^o$ the influence of pressure port purging on the local flow behaviour is examined.

INTRODUCTION

Multi-hole pressure probes are used to measure fluid static and total pressure, along with the mean fluid velocity and direction (Bryer and Pankhurst, 1971). Several probe geometries have been used to measure 3D flows, including hemispherical and spherical shaped probes (Wright, 1970), and conical tip probes (Judd 1975, Everett et al. 1983). The number of pressure holes on the probe tip varies, with Wright using five holes and Everett and co-workers working with a seven hole probe. A common configuration is a five hole pressure probe, composed of five tubes interconnected to form a solid tip. In order to minimize the flow disturbance and maximize the resolution, the probes are made relatively small, with five hole pressure probes usually around 2 to 3 mm in diameter. Ligrani et al. (1989) discuss miniature five hole pressure probes with tip diameters of about 1.22 mm, used in small confined areas and where the scales of turbulence are also small.

The particular probe to be investigated is the four-hole Cobra pressure probe originally proposed by Shepherd (1981). This probe has a tip shaped like the frustrum of a pyramid (Figure 1). Three side holes surround a fourth central hole, with the three side faces ground flat to 45 degrees. The shaft has a 'J' shape that maintains the probe tip at a fixed point whilst rotating about the shaft axis. Shepherd also discusses the relative merits of the four-hole Cobra probe as opposed to using five or more pressure ports. Figure 1 illustrates the two flow angles that are used to define the fluid flow direction.

The Cobra probe measures flow quantities using a calibration technique. Extensive calibration data has been generated for this probe, its usage extending to flows up to 110 m/s, within a yaw and pitch angle range of +- 48 degrees (Hooper and Musgrove, 1991). Their paper also demonstrates the use and effectiveness of the probe in a typical industrial flow situation, namely in a highly turbulent wake region.

It is proposed to use the probe in particle laden flows. To prevent blockage of the pressure ports by the particles, a mass flow rate of air coming out of the pressure holes could be used to purge the holes.

The purpose of this paper is to investigate, using Computational Fluid Dynamics (CFD), the detailed flow behaviour around the probe tip for representative angles of operation. Purging gas through the holes will also be modelled, to see whether this significantly affects the local flow behaviour, and hence the sensitivity of the probe pressure response to varying purging flow rates. The investigation will also yield the pressure response of the probe at various pitch and yaw angles of the flow, enabling a measure of comparison between the calibration data of Hooper and Musgrove (1991) and the present computational simulation.

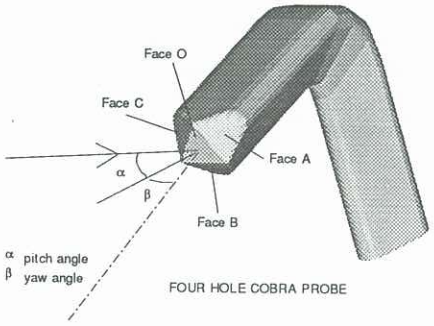

Figure 1. Cobra probe and flow angles

CFD CODE AND GRID GENERATION

The CFD code to be used is described below, with emphasis on the fact that this code is a very general piece of software that can solve a large variety of industrial type flows. An outline of the procedures employed in generating the computational grid will also be given.

The fluid flow around the probe is solved using a CFD code, RANSTAD (Reynolds Averaged Navier Stokes Solver for Aerodynamic Design). RANSTAD was developed for complex industrial flows , and is suitable for laminar or turbulent flows, in 2D or 3D. It handles both incompressible and compressible flows, and can also solve for temperature, enthalpy and two-phase behaviour (Fletcher, 1991a). It can be applied to internal geometries such as the flow through ducts and flow machinery, and external flows ie. around wing body junctions, automobiles and buildings. RANSTAD uses a k-ε turbulence model or an algebraic Reynolds stress turbulence model (ASM) to provide the Reynolds stress predictions (Rodi, 1980). A one or two-layer wall function (Armfield et al, 1990) is implemented with these models to avoid the need for very fine grids adjacent to solid surfaces. A higher order finite volume discretisation scheme (Cho et al, 1990) with inbuilt limiters combines robustness with higher-order accuracy on relatively coarse grids.

The code uses a non-orthogonal boundary fitted coordinate grid system (Thompson et al, 1985). The momentum equations are solved for the velocity components on a non-staggered grid ie. all variables U,V,W,P are stored at the centroids of the mass control volumes.

First order derivatives in the governing equations are evaluated using four-point asymmetric discretisation (Fletcher, 1991b) to retain high accuracy in coarse grids. Each governing equation is sequentially relaxed to update one of the primitive variables. A velocity potential correction is introduced to satisfy continuity and upgrade the pressure using a modified SIMPLEC algorithm (Van Doormal and Raithby, 1984). The Rhie-Chow (1983) momentum interpolation method is used to prevent chequerboard oscillations in pressure. A strongly implicit procedure (SIP) scheme is used to upgrade the velocity components and the velocity potential.

The CFD code used to solve the 3D fluid flow around this probe required a structured, single block grid (Eriksson, 1987) in a body fitted coordinate system. Therefore the computational grid is referred to as being topologically cuboidal.

The 3D grid is constructed by stacking 2D grid planes, these planes being slices through the probe cross-sectional area. Stacking of surfaces have been used widely ie. in papers by Chang (1983), Chen et al (1982), and Holst and Thomas (1983).

On each 2D slice, the multisurface method (Eiseman, 1979) is applied to twelve separate blocks or sections of the grid. The multisurface method is used with two intermediate surfaces, one of which is adjacent to the probe surface to produce a grid which is locally near-orthogonal to the solid body. The bounding curves defining the domain and the solid surfaces are represented by Hermite splines (Kahaner, 1989). Grid point clustering is accomplished by distributing the points along the bounding curves using one-dimensional stretching functions (Roberts 1971, Eiseman 1979).

After stacking the 2D grid slices to form the 3D grid, the existing grid has a large number of regions where grid overlap and highly skewed grid cells occur. This seems to be a common occurrence in 3D grid generation methods, especially where 2D grids are combined to form 3D grids (Kennon and Dulikravich 1986, Thompson 1984). Here the existing grid is improved in terms of smoothness and orthogonality by applying an elliptic generation system based on the Laplace equations (Thompson et al 1985, Warsi 1982). A sample grid is shown in Figure 2.

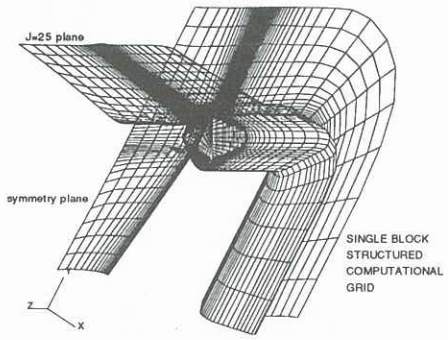

Figure 2. Computational grid

RESULTS

The computations were obtained on a 44x39x57 grid, with each case requiring approximately 1000 global iterations to reduce the rms residuals to below $1x10^{-9}$. A uniform velocity profile of 16 m/s is imposed on the probe, with the corresponding Reynolds number based on the tip width equal to 2×10^3. A laminar model is then used to calculate the flow around the probe tip. The pressure ports are modelled by including 32 control volumes inside each pressure hole, and then imposing Dirichlet boundary conditions for the flow rate in the interior of these holes.

Detailed flow solutions will be presented for the cases where the pitch angle is kept at 0^o and the yaw angle is varied between 0^o and 48^o. This will illustrate representative cases of the probe's operation wherein some of the pressure faces are exposed to the incoming flow and some are rearward facing with respect to the flow.

Figures 3, 4 and 5 show the 2D velocity vectors in the plane of symmetry of the probe as the yaw changes between 0^o, 15^o and 48^o respectively. Figure 3 shows that in the case pitch=0^o, yaw=0^o, only a very small region of separation occurs at the top of the probe, but a large recirculating region exists at the bottom side after the flow has gone past face B. The vectors at the top of the probe shows the rapid change in velocity as one moves away from the solid surface, showing the extent of the boundary layer. When the yaw angle is changed to 15^o, this recirculating region at the bottom of the probe disappears (Figure 4), with the fluid now flowing smoothly past the curved sides of the probe. Now the top of the probe shows considerable separation, with the flow going past face A. Note that the recirculating region is not confined to the plane of symmetry, but is a 3D vortex that propagates into the direction of the page.

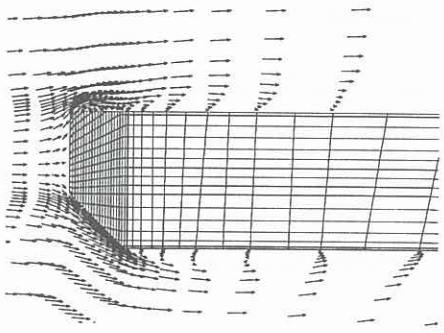

Figure 3. Velocity vectors Pitch=0^o Yaw=0^o

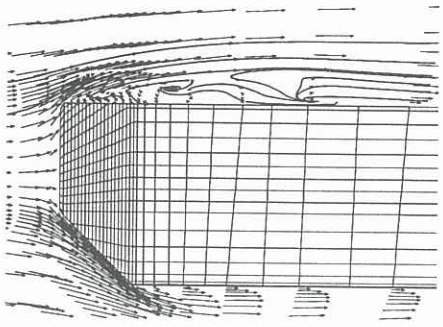

Figure 4. Velocity vectors and streamlines Pitch=0^o Yaw=15^o

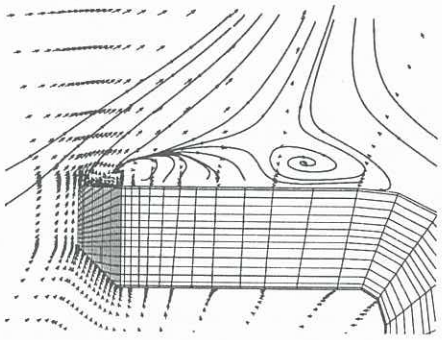

Figure 5. Velocity vectors and streamlines Pitch=0^o Yaw=48^o

At a yaw angle of 30^o the flow solution is very similar to the yaw=15^o case, with the separation region (in the plane of symmetry) being slightly shorter as measured from the front of the probe.

When the yaw angle is increased to 48^o (Figure 5), a markedly different flow pattern results. Now the stem of the probe has a large influence on the flow behaviour near the tip. A vortex is formed where the flow past the tip meets with the flow past the bend in the stem.

Looking now at the horizontal plane represented by the grid coordinate J=25 (see Figure 2), the flow solution is shown in Figure 6 for the pitch=0^o yaw=0^o case and in Figure 7 for the pitch=0^o yaw=20^o case. Figure 6 shows a small amount of separation occurring at the sides of the probe after the flow has left the faces. As the yaw angle is increased to 20^o, the separation region becomes more pronounced on the downstream side, and does not exist on the windward side. When the yaw angle is increased to 48^o , flow separation occurs off pressure face C. This separation of the face is not present for yaw angles less than 30^o.

The pressure solution on this plane is illustrated in Figure 8 for the yaw angles 0^o, 15^o and 30^o. The pressure contours show the shift in the stagnation point as the yaw angle is changed, and the appearance of low pressure regions on the leeward sides.

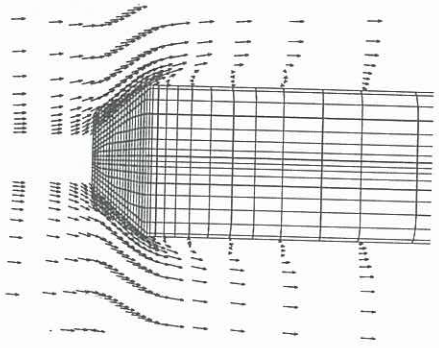

Figure 6. Velocity vectors Pitch=0° Yaw=0°

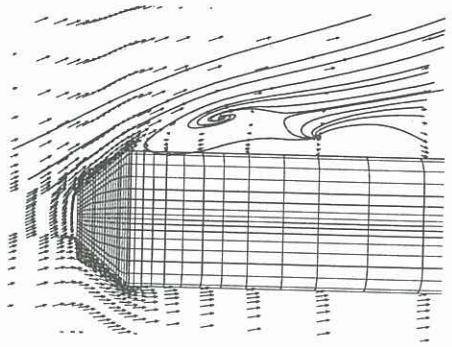

Figure 7. Velocity vectors and streamlines Pitch=0° Yaw=20°

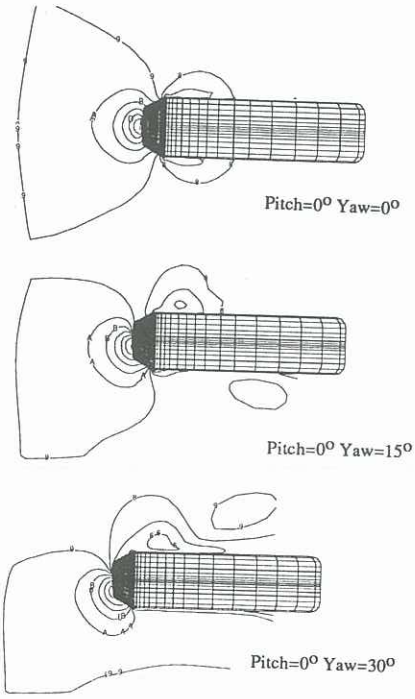

Figure 8. Pressure contours

Comparison to experimental calibration

Figure 9 is a graph comparing the pressure readings of the various probe holes, done in a similar fashion to Hooper and Musgrove (1991). The pitch angle is at 42°, with the yaw angle varying. Their calibration data is represented by the symbols, and the computational results of RANSTAD are shown by the solid lines. Good agreement is apparent for the higher pressures, but discrepancies are present for the lower pressure readings, which of course correspond to the pressure ports on the leeward faces where separation is occurring. For a lower pitch angle, say the zero pitch case, the computational results agree much better with the experimental calibration for all yaw angles. At the higher pitch and yaw angles, the computational model perhaps fails to match exactly the near wall flow behaviour where separation occurs, therefore the pressure solution in the separation region is slightly different.

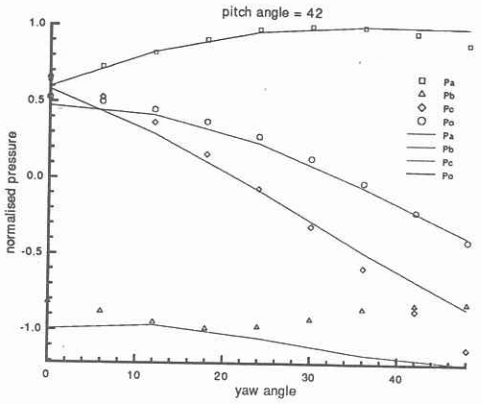

Figure 9. Calibration graph

An improvement to this discrepancy could be brought about by putting more grid points in these regions, with the corresponding increase in computational resources required. At the same time, a computational model that followed the geometry of the actual probe more closely would result in determining the exact point of separation, thus leading to a more accurate pressure solution. Figure 10 shows the near tip flow behaviour for the case pitch=42° yaw=36°. A critical feature of the probe geometry illustrated in this figure is the amount of curvature present at the edge of the faces. Modelling the actual radius of curvature will shift the point and extent of the separation, leading to a more accurate representation of the flow.

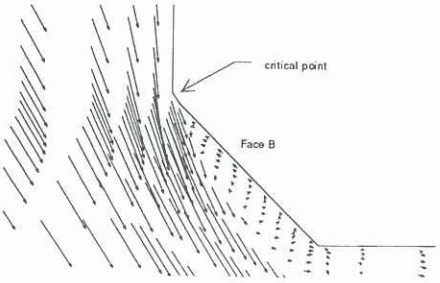

Figure 10. Velocity vectors Pitch=42° Yaw=36°

Gas purging cases

The results presented for the cases where gas is blown out of the pressure ports are restricted to one fixed orientation of the probe, namely the pitch=0° yaw=20° case, while the gas flow rate is varied. The purging gas is blown in the hole axial direction only, and the flow rate of purging is the same in all four holes.

Figure 11 shows the velocity solution in the horizontal (J=25) plane. Here the purging rate is 12 m/s. The zero purging rate solution is shown in Figure 7. The downstream side yields a separation region where vortices have formed. There is a vortex very near the pressure port, indicating that the influence of the purging gas is restricted to near the tip only. This changes as the purging rate is increased.

Figure 12 shows the solution when the purging rate is 18 m/s. A large recirculating region has formed, with the purging gas coming out of the leeward port turning smoothly under the influence of the approaching flow. The flow forms a vortex, with the streamlines showing that some of the fluid inside the vortex being entrained back into the purging gas flow region.

When the purging rate is increased to 38 m/s, (see Figure 13) the influence of the purging gas extends further out into the approaching flow, as evidenced by the standing vortex that is formed quite a distance away from the pressure port.

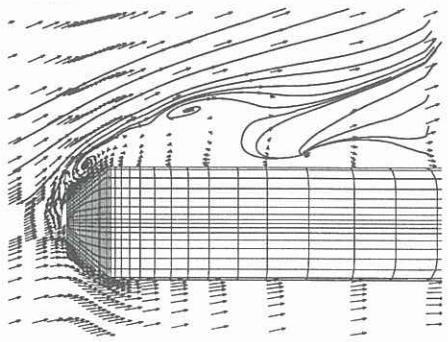

Figure 11. Velocity vectors and streamlines Pitch=0° Yaw=20° Gas=12

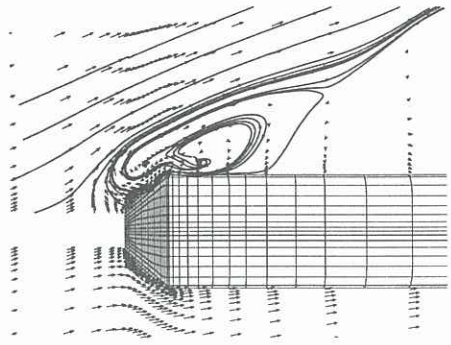

Figure 12. Velocity vectors and streamlines Pitch=0° Yaw=20° Gas=18

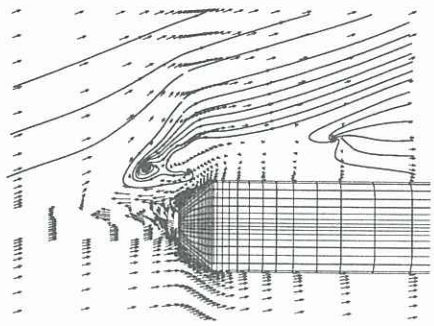

Figure 13. Velocity vectors and streamlines Pitch=0° Yaw=20° Gas=38

It is instructive to note that in all these cases, the flow behaviour on the upstream side of the probe is hardly different to the non-purging case. The influence of the purging gas on the approaching flow is not significant, and a higher rate of purging might be required to effectively prevent and/or clear blockage by solid particles on the windward faces.

The pressure solution for a purging rate of 28 m/s is shown in Figure 14. The purging gas has caused severe pressure gradients in the vicinity of the pressure ports, and this might cause an uncertain pressure reading when the probe is in operation.

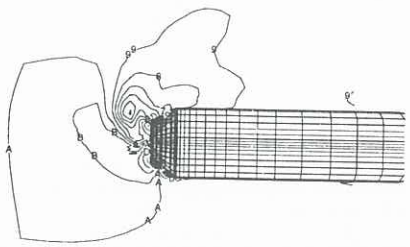

Figure 14. Pressure contours Pitch=0° Yaw=20° Gas=28 m/s

CONCLUSION

The fluid flow around the four-hole Cobra probe has been investigated computationally, revealing some complicated flow behaviour that occurs near the tip. Comparison between the computational results and the experimental calibration data show good agreement for the cases where the pitch and yaw angles are small, with discrepancies occuring when the probe is oriented such that flow separation behaviour influences the pressure solution. The influence of purging gas on the local flow behaviour has also been presented.

ACKNOWLEDGMENT

The first author is supported by an Australian Postgraduate Research Award and a scholarship from CSIRO Division of Mineral and Process Engineering. Their support is gratefully acknowledged.

REFERENCES

ARMFIELD, S.W., CHO, N-H and FLETCHER, C.A.J. (1990), *A.I.A.A. J.*, **28**, 453-460

BRYER, D.W. and PANKHURST, R.C. (1971) *Pressure-probe Methods for Determining Wind Speed and Flow Direction.* H.M.S.O.

CHANG, I.S. (1983) Three-dimensional, two-phase supersonic nozzle flows, *A.I.A.A. J.*, **21**, 671

CHEN, B.C-J., CHIEN, T.H., SHA, W.T. and KIM, J.H. (1982) 3-D solution of flow in an infinite square array of circular tubes by using boundary-fitted coordinate systems. *Numerical Grid Generation*, ed. by J.F. Thompson, North-Holland, 1982

CHO, N-H, FLETCHER, C.A.J. and SRINIVAS, K. (1990) Efficient computation of wing body flows. 12th Int. Conf. Num. Meth. Fluid Dynamics, Oxford, U.K., June 1990

EISEMAN. P.R. (1979) A multi-surface method of coordinate generation. *J. Comp. Phys.*, **33**, 118-150

ERIKSSON, L-E. (1987) Flow solution on a dual-block grid around an airplane. *Comput. Meths. Appl. Mech. Engrg 64*, 79-93

EVERETT, K.N., GERNER, A.A. and DURSTON, D.A. (1983) Seven-hole cone probes for high angle flow measurement: theory and calibration. *A.I.A.A. J*, **21**, 992-998

FLETCHER, C.A.J. (1991a) Computational modelling of complex industrial flows. 4th Int. Symposium on Transport Phenomena, ISTP-IV (ed. J.A. Reizes), Sydney, July 1991

FLETCHER, C.A.J. (1991b) *Computational Techniques for Fluid Dynamics.* 2nd Edn. Springer-Verlag

HOLST, T. and THOMAS, S. (1983) Numerical solution of transonic wing flow fields. *A.I.A.A. J.*, **21**, 863

HOOPER, J.D. and MUSGROVE, A.R. (1991) Multi-hole pressure probes for the determination of the total velocity vector in turbulent single-phase flow. 4th Int. Symposium on Transport Phenomena, ISTP-IV (ed. J.A. Reizes), Sydney, July 1991

JUDD, A.M. (1975) Calibration of a five tube probe for measuring wind speed and direction. *J. Phys E:Sci. Instrum.*, **8**, 115-116

KAHANER, D., MOLER, C. and NASH, S. (1989) *Numerical Methods and Software.* Prentice-Hall

KENNON, S.R. and DULIKRAVICH, G.S. (1986) Generation of computational grids using optimization. *A.I.A.A. J.*, **24**, 1069-1073

LIGRANI, P.M., SINGER, B.A. and BAUN, L.R. (1989) Miniature five-hole pressure probe for measurement of three mean velocity components in low-speed flows. *J Phys E:Sci. Instrum.*, **22**, 868-876

RHIE, C.M. and CHOW, W.L. (1983) Numerical study of turbulent flow past an airfoil with trailing edge separation. *A.I.A.A. J.*, **21**, No.11, 1525-1532

ROBERTS, G.O. (1971) Lecture Notes in Physics, Vol. 8 (Springer, Berlin, Heidelberg) 171-176

RODI, W. (1980) *Turbulence Models and Their Application in Hydraulics* (I.A.H.R., Delft)

SHEPHERD, I.C. (1981) A four-hole pressure probe for fluid flow measurements in three dimensions. *J Fluids Engineering*, **103**, 590-594

THOMPSON, J.F. (1984) Grid generation techniques in computational fluid dynamics. *A.I.A.A. J.*, **22**, 1505-1523

THOMPSON, J.F., WARSI, Z.U.A. and WAYNE MASTIN, C. (1985) *Numerical Grid Generation*, North-Holland

VAN DOORMAL, J.P. and RAITHBY, G.D. (1984) Enchancements for the SIMPLE method for predicting incompressible fluid flow. *Num. Heat Transfer*, **7**, 147-163

WARSI, Z.U.A. (1982) Basic differential models for coordinate generation. *Numerical Grid Generation*, ed. by J.F. Thompson, North-Holland, 1982

WRIGHT, M.A. (1970) The evaluation of a simplified form of presentation for five-hole spherical and hemispherical pitometer calibration data. *J Phys E:Sci. Instrum.*, **3**, 356-362